Characterization of the Methoxy Carbonyl Radical Formed via Photolysis of Methyl Chloroformate at 193.3 nm

M. J. Bell, K.-C. Lau,† M. J. Krisch,‡ D. I. G. Bennett, and L. J. Butler*

The James Franck Institute and Department of Chemistry, The University of Chicago, Chicago, Illinois 60637

F. Weinhold

Department of Chemistry, University of Wisconsin, Madison, Wisconsin 53706

Received: September 16, 2006; In Final Form: December 4, 2006

This study investigates two features of interest in recent work on the photolytic production of the methoxy carbonyl radical and its subsequent unimolecular dissociation channels. Earlier studies used methyl chloroformate as a photolytic precursor for the CH_3OCO, methoxy carbonyl (or methoxy formyl) radical, which is an intermediate in many reactions that are relevant to combustion and atmospheric chemistry. That work evidenced two competing C−Cl bond fission channels, tentatively assigning them as producing ground- and excited-state methoxy carbonyl radicals. In this study, we measure the photofragment angular distributions for each C−Cl bond fission channel and the spin−orbit state of the Cl atoms produced. The data shows bond fission leading to the production of ground-state methoxy carbonyl radicals with a high kinetic energy release and an angular distribution characterized by an anisotropy parameter, β, of between 0.37 and 0.64. The bond fission that leads to the production of excited-state radicals, with a low kinetic energy release, has an angular distribution best described by a negative anisotropy parameter. The very different angular distributions suggest that two different excited states of methyl chloroformate lead to the formation of ground- and excited-state methoxy carbonyl products. Moreover, with these measurements we were able to refine the product branching fractions to 82% of the C−Cl bond fission resulting in ground-state radicals and 18% resulting in excited-state radicals. The maximum kinetic energy release of 12 kcal/mol measured for the channel producing excited-state radicals suggests that the adiabatic excitation energy of the radical is less than or equal to 55 kcal/mol, which is lower than the 67.8 kcal/mol calculated by UCCSD(T) methods in this study. The low-lying excited states of methylchloroformate are also considered here to understand the observed angular distributions. Finally, the mechanism for the unimolecular dissociation of the methoxy carbonyl radical to $CH_3 + CO_2$, which can occur through a transition state with either cis or, with a much higher barrier, trans geometry, was investigated with natural bond orbital computations. The results suggest donation of electron density from the nonbonding C radical orbital to the σ^* orbital of the breaking C−O bond accounts for the additional stability of the cis transition state.

I. Introduction

As the environmental effects of energy acquisition become more apparent, the need for more efficient fuels is increasing. Concerns about combustion byproducts including soot and greenhouse gases necessitate the development of cleaner combustion mechanisms. Studies on the dynamics and the energetics of combustion reaction intermediates provide vital information to facilitate this development. The methoxy carbonyl radical is an intermediate in many combustion and atmospheric chemical reactions including the methoxy + CO reaction[1−3] (which is integral to the methane combustion mechanism), the combustion and atmospheric oxidation of dimethyl ether,[4,5] and the combustion of dimethyl carbonate.[6] Of particular interest in the above reactions is the development of oxygenated fuels that hinder soot production by forming CO and CO_2 as combustion products. Numerous theoretical and experimental studies have investigated the methoxy carbonyl radical as an intermediate in the oxidation of dimethyl ether, which is currently being investigated as an additive to conventional diesel fuels to reduce soot formation. Most studies have focused on the production of the methoxy carbonyl radical from the reaction of methyl formate with Cl,[7−9] H and methyl,[10] and hydroxyl[4,11] radicals.

The reaction of CH_3O with CO and the unimolecular dissociation of the methoxy carbonyl radical intermediate has been investigated extensively with a wide range of theoretical methods. Early theoretical work[1,12−14] suggested that the dissociation of the radical to form $CH_3O + CO$ proceeded by a lower barrier (∼21 kcal/mol) than the barrier (∼32 kcal/mol) to the more exothermic $CH_3 + CO_2$ product channel, leading to the prediction that the product branching in the unimolecular dissociation of this radical under collision-free conditions would be dominated by $CH_3O + CO$. In the most complete study, incorporating a model for collisional stabilization of the radical intermediates, Wang et al.[13] used the G2(B3LYP/MP2/CC) method to study the $CH_3O + CO$ reaction and performed Rice−Ramsperger−Kassel−Markus calculations to predict the

* Corresponding author. E-mail: l-butler@uchicago.edu.
† Present address: Dept. of Biology and Chemistry, City University of Hong Kong, Kowloon, Hong Kong.
‡ Present address: Department of Chemistry and AirUCI, University of California at Irvine, CA 92697.

10.1021/jp066056i CCC: $37.00
Published on Web 02/20/2007

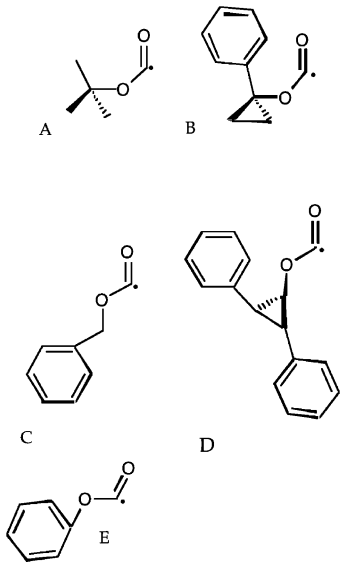

Figure 1. Selected alkyl formate radicals shown to undergo unimolecular dissociation via CO_2 loss.

products of the multiwell reaction as a function of temperature and pressure. Good et al.[5] also published barriers computed at the G2 level of theory for the unimolecular dissociation of the methoxy carbonyl radical but obtained a much lower barrier, 14.7 kcal/mol, to the $CH_3 + CO_2$ product channel than those predicted by the work of Francisco et al.,[1] Kang and Musgrave,[12] Wang et al.,[13] and Zhou et al.[14] In crossed laser-molecular beam studies of the $CH_3O + CO$ system, McCunn et al.[15] measured product branching ratios under collision-free conditions for the unimolecular dissociation of the CH_3OCO radical. The experimental results are in dramatic disagreement with predictions using the earlier high barrier calculated for the dissociation of methoxy carbonyl to methyl + CO_2 but in good agreement with the predicted branching ratio using the low barrier height of 14.7 kcal/mol predicted by Good et al.[5] for the formation of $CH_3 + CO_2$. Subsequent CCSD(T) studies[15] on the unimolecular dissociation of methoxy carbonyl indicated that the lower barrier to the methyl + CO_2 products results from a cis geometry of the transition state (*cis*-TS), whereas the higher barrier corresponds to a trans conformation at the transition state (*trans*-TS). The present work seeks to gain an understanding of why the barrier from the cis conformer is so much lower than that from the trans conformer.

Interestingly, although there has been some disagreement about the barrier energies of the product channels for the unimolecular dissociation of methoxy carbonyl radical, there is general agreement that the main dissociation pathway for larger alkoxy carbonyl radicals (see Figure 1) in bulk experiments is CO_2 elimination.[16−18] Ab initio calculations[19] at the CCSD(T)/aug-cc-pVDZ//MP2/aug-cc-pVDZ level of theory supported the experimental results, with calculated barriers of 16.8, 17.4, 16.0, and 14.4 kcal/mol for the decarboxylations of methoxy carbonyl, ethoxy carbonyl, *iso*-propoxy carbonyl, and *tert*-butoxy carbonyl radicals, respectively. The calculations clearly indicate a correlation between the stability of the alkyl radical leaving group and the barrier height. The barrier of 16.8 kcal/mol for CO_2 production from the methoxy carbonyl radical is slightly higher than the barrier presented by McCunn et al.[15] but still lower than the predicted barrier to dissociate to $CH_3O + CO$. Note also that recent calculations at the B3LYP/6-311++G(d,p) level of theory on sulfur analogues found that the CH_3OSO dissociation barrier to $CH_3 + SO_2$, 37.3 kcal/mol,[20] is lower in energy than the barrier to form $CH_3O + SO$.

Kinetic modeling studies performed by Westbrook et al.[21] indicate that upon combustion the ester moieties present in biodiesel fuel alternatives proceed though larger alkoxy carbonyl radicals (analogous to the methoxy carbonyl radical) to produce CO_2. Other work by Glaude et al. on the combustion of dimethyl carbonate,[6] also under consideration as a fuel additive, developed a kinetic mechanism for the reaction, which incorporated the methoxy carbonyl radical. The mechanism of Glaude et al. indicates that most of the oxygen in the dimethyl carbonate goes into the direct production of CO_2 via dissociation of the methoxy carbonyl radical. Both Glaude[6] and Westbrook[21] remark that direct production of CO_2 in the combustion of oxygenated fuels is not an ideal utilization of oxygen because only one C atom per every two O atoms has been prevented from forming carbon−carbon bonds that characterize soot precursors.

As noted above, McCunn et al.[15] tentatively concluded that a low-lying excited-state of the methoxy carbonyl radical, at most 55 kcal/mol higher in energy than the ground-state radical, is produced in one of the unimolecular photodissociation channels of methyl chloroformate at 193.3 nm. Although there has been a bevy of published research on the ground state of the methoxy carbonyl radical, there is relatively little published work on the excited state of the radical implicated in the experimental results of McCunn. Hansen et al.[22] reported the vertical excitation energies for the methoxy carbonyl radical and the corresponding UV spectra. Multireference configuration interaction methods using the aug-cc-pVDZ basis set yielded vertical excitation energies of 99.93 kcal/mol ($1\ ^2A' \rightarrow 1\ ^2A''$), 106.40 kcal/mol ($1\ ^2A'' \rightarrow 2\ ^2A''$), 127.57 kcal/mol ($1\ ^2A' \rightarrow 2\ ^2A'$), and 145.38 kcal/mol ($1\ ^2A' \rightarrow 3\ ^2A'$).

The present work probes two key features of the methoxy carbonyl radical; the first relates to the photolytic production of methoxy carbonyl from methyl chloroformate, and the second relates to the radical's unimolecular dissociation dynamics. The experimental production of methoxy carbonyl radicals in two states (tentatively assigned to the ground and first excited state) via the phtotodissociation of methyl chloroformate by 193.3 nm light is examined here by analyzing the angular distributions of the products from the two C−Cl bond fission channels. We interpret the results with preliminary excited-state calculations on the methyl chloroformate potential energy surface to see if indeed two excited states of methyl chloroformate are dissociating to yield two different electronic states of methoxy carbonyl radical. High-level ab initio calculations of the adiabatic excitation energy of the methoxy carbonyl radical are also compared to the minimum internal energy measured by McCunn et al.[15] for the high internal energy species produced in the photolysis of methyl chloroformate. We then turn to a theoretical analysis of the dramatically different predictions for the product channel barrier heights for the unimolecular dissociation of methoxy carbonyl to produce methyl + CO_2 via a cis transition state and a higher-energy trans-geometry transition state. A natural bond orbital analysis identifies the dominant manifold interactions that result in the cis transition state being lower in energy. These qualitative results provide insight into the experimental observation of the product branching ratios in the system.

II. Experimental and Computational Methods

A. Experimental Details. The angular distribution and velocity distribution of the Cl fragments is determined from the time-of-flight distribution of the nascent species produced by photodissociating methyl chloroformate with polarized light utilizing a crossed laser-molecular beam apparatus. The details

of the crossed laser-molecular beam apparatus have been described thoroughly in prior publications,[23] and only the important points will be covered in the present work. UV light (193.3 nm) corresponding to the ArF transition from a pulsed Lumonics Pulsemaster PM 848 Excimer laser operating at 100 Hz passes first through a Spectra Physics single-crystal quartz birefringent Pelin-Broca crystal that separated the unpolarized laser beam into two linearly polarized beams. The horizontally polarized beam then passes through a half-wave retarder to permit the angle of polarization to be varied. In advance of the experiments, the optical purity of the light and the alignment of the optic axis in the half-wave retarder are verified using a second birefringent Pelin-Broca crystal.

The now polarized light, with powers ranging from 4 to 6 mJ/pulse, is focused to a 2×2.5 mm^2 spot at the interaction region of a differentially pumped chamber where the laser light photodissociates a molecular beam of methyl chloroformate set at a 15° source angle. The 9.5% methyl chloroformate beam is created by bubbling a He carrier gas (with a total backing pressure of 315 Torr) through methylchloroformate (99% purity, Aldrich) cooled to −7.7 °C and expanded supersonically through an 0.004 in diameter nozzle held to about 200 °C. Some of the scattered photofragments travel through the 1.5° acceptance angle of the detector and are ionized by 200 eV electrons. From there, a quadrupole mass spectrometer allows only $m/e = 35$ ions (corresponding to an ionized ^{35}Cl fragment) to pass to a Daly detector. The $m/e = 35$ data presented in this paper was collected at six polarization angles (the angle between the polarization vector of the laser light and the line from the crossing point of laser and molecular beam to the detector) for a total of 4.5×10^5 shots at each angle.

Additional two-dimensional photofragment imaging experiments are undertaken to determine the translational energy distributions of each spin−orbit state of the chlorine atoms produced in the photolysis of methylchloroformate. Again, the details of this apparatus have been discussed thoroughly in prior literature.[24,25] Helium gas is bubbled through liquid methyl chloroformate at 5 °C and passes through a pulsed nozzle and supersonically expands in the interaction region of a differentially pumped vacuum chamber. The resulting molecular beam is photolyzed by 193.3 nm light from a GAM ArF excimer EX10F/300 laser operating at 20 Hz. The atomic Cl($^2P_{1/2}$) and Cl($^2P_{3/2}$) photofragments are ionized using [2 + 1] resonance-enhanced multiphoton ionization (REMPI) at 235.20 and 235.34 nm, respectively. The 235 nm light is obtained by combining 706 nm light (produced from an Nd:YAG pumped Lambda Physik FL3002 dye laser using LDS698 dye) and 353 nm light (produced via frequency doubling the dye laser output light in a KDP crystal) in a BBO crystal. Following ionization, the ion cloud accelerates toward a two-dimensional position-sensitive detector. The ions are detected using a Burle 3040FM detector consisting of a chevron multichannel plate (pulsed to −750 V with a pulse width of 80 ns) coupled to a P20 phosphor screen (held at 3.5 kV above the final plate of the MCP). A 1376 × 1040 pixel La Vision Imager 3 pixel charged coupled device camera records the images on the phosphor screen. The event counting method[26] incorporating the algorithm in the DaVis imaging software is used to obtain the photofragment signal.

B. Theoretical Details. Calculations are performed on both the methoxy carbonyl radical and its photolytic precursor, methyl chloroformate. The adiabatic excitation energy between the ground and first excited states of the methoxy carbonyl radical is studied using restricted Hartree−Fock (RHF) based unrestricted coupled-clusters including single, double, and perturbative triple excitations [UCCSD(T)]. A cc-pVTZ basis set is used for calculations involving the radical. Symmetry is invoked during the geometry optimization on the excited-state surface, but the ground-state radical is allowed to optimize to a slightly out-of-plane equilibrium geometry. For methyl chloroformate, preliminary calculations are undertaken using state-averaged multiconfiguration self-consistent field theory (SA-MCSCF) with a cc-pVDZ basis set. The active space consisted of 22 occupied A′ orbitals with 8 active A′ orbitals containing 5 electrons and 6 A″ orbitals with 5 active A″ orbitals containing 8 electrons. The ground-state geometry for each conformer was optimized without state-averaging. Symmetry was invoked for the geometry optimization on the ground state and the calculation of the vertical excitation energies. For computational ease, the calculations of the transition moments included only three states in a given calculation, the ground state and two excited states (either both A′ or A″). MOLPRO[27] 2002.6 was used for all calculations.

We also performed calculations to examine the dissociation pathways of the methoxy carbonyl radical to $CH_3 + CO_2$. To study the relatively large energetic difference between the *cis*-TS and *trans*-TS, we carried out a natural bond orbital (NBO)[28−30] analysis along the potential energy surface for the dissociation of *cis*-/*trans*-methoxy carbonyl radicals into $CH_3 + CO_2$ via the respective *cis*-TS and *trans*-TS. The potential energy surfaces are constructed by scanning the intrinsic reaction coordinate (IRC) of the *cis*-TS and *trans*-TS in both reverse and forward directions using the Gaussian 03 program, and the relative energetics for both pathways are plotted against the C−O bond length (R) of the dissociating CH_3−OCO. The potential energy surfaces are evaluated at the B3LYP/6-311G-(2df,p) level of theory. Along the potential energy surface of *cis*-/*trans*-CH_3OCO en route to formation of *cis*-TS and *trans*-TS, we selected several IRC points (R = 1.46, 1.49, 1.60, 1.70, 1.75 and 1.84 Å) on the surfaces for NBO analysis with the GENNBO 5.0W software.[31]

III. Results and Discussion

A. Photofragment Angular Distribution Data. The resulting TOF spectra at $m/e = 35$ for the six polarization angles are consistent with the results in McCunn et al.[15] and are fit with the C−Cl bond fission recoil translational energy distributions derived from fits to the data in that work (Figure 2). To determine the angular distribution as a function of laser polarization angle, the spectra at each angle are integrated separately over time windows corresponding to the photodissociation signal as seen in Figure 3. Separate integrations of the signal from the high kinetic energy C−Cl bond fission channel (identified by McCunn et al.[15] as the ground-state product channel) and the signal from the low kinetic energy C−Cl bond fission channel (identified by McCunn et al.[15] as the excited-state product channel) are performed so that anisotropy parameters for each channel can be determined individually. From the separate integrations of the Cl signal, the product branching ratios of the channels producing excited- and ground-state radicals are evaluated. Branching fractions of 0.82 for the production of ground-state methoxy carbonyl radical and 0.18 for the production of excited-state methoxy carbonyl radical are determined. This branching fraction includes a correction for the different angular distributions of photofragments for each channel. We describe this correction to the branching fraction in section III.F of this paper.

The classical electric dipole equation (eq 1), where θ_{cm} is the angle between the electric vector of the linearly polarized

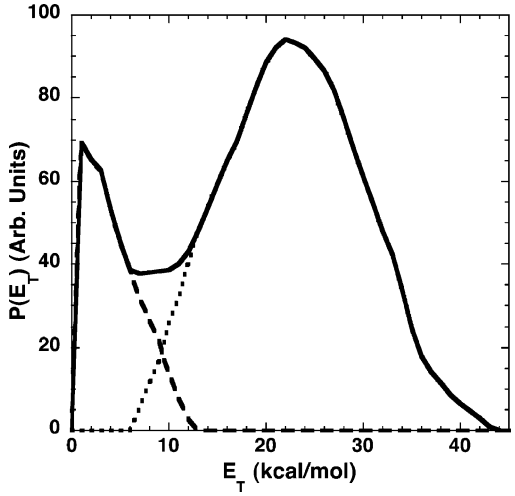

Figure 2. Total recoil translational energy distributions in the C−Cl bond fission channels from McCunn et al.[15] used to fit our polarization data. The dashed line represents the channel resulting in excited methoxy carbonyl radical products, and the dotted line represents the channel forming ground-state methoxy carbonyl products. The solid line is the total $P(E_T)$. This figure is adapted with permission from Figure 4 in ref 15.

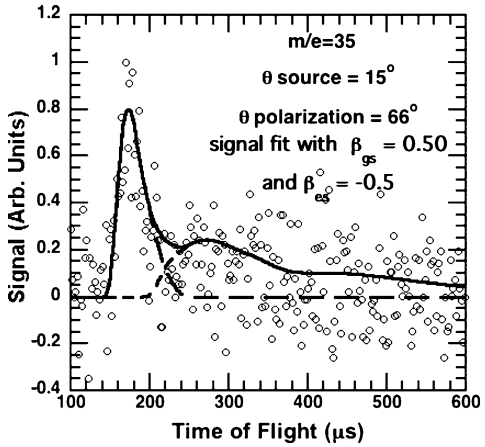

Figure 3. Cl time-of-flight spectrum taken at a polarization angle of $\theta = 66°$ between the electric vector of light and the scattering axis. The source angle is 15°. The bimodal spectrum is fit with two translational energy distributions $P(E_T)_{EX}$ (corresponding to the slow peak) and $P(E_T)_{GR}$ (corresponding to the fast peak); the dissociation channels corresponding to each of these $P(E_T)$s exhibit different anisotropy parameters.

light and the fragments' recoil direction in the center of mass reference frame and P_2 is the second-degree Legendre polynomial, characterizes the angular distribution of the Cl atoms measured in our experiments and can be used to determine β, the anisotropy parameter.[32,33]

$$I(\theta_{cm}) = \frac{1}{4\pi}[1 + \beta P_2(\cos\theta_{cm})] \quad (1)$$

For ease of analysis, eq 1 was modified for use in the lab reference frame. A forward convoluting data-fitting program takes the molecular beam velocity distribution, source−detector angle, and corrected branching fraction into account and uses the previously determined empirical $P(E_T)$ (Figure 2) to fit the data. The anisotropy parameter β is varied to obtain a good fit to the integrated data. Our data is best fit by an anisotropy parameter of $\beta = 0.50$ with the 95% confidence interval ranging from $\beta = 0.37$ to $\beta = 0.64$ for the high kinetic energy C−Cl fission channel. The signal from the low kinetic energy C−Cl

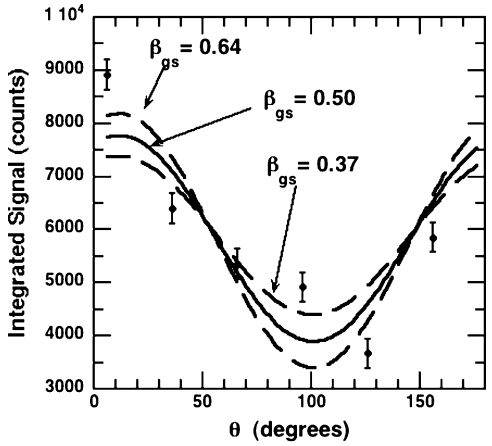

Figure 4. Angular distribution of the Cl fragments formed in the high recoil kinetic energy channel following photolysis of methyl chloroformate. The portion of the Cl signal integrated from 154 to 234 μs is plotted as a function of the lab polarization angle between the electric vector of the laser and the line from the interaction region to the detector. The integration range corresponds to the fast peak in each TOF distribution (e.g., see Figure 3); these C−Cl bond fission events produced ground-state methoxy carbonyl radicals. The experimental data (solid circles) are shown with $\pm\sigma$ error bars. The best fit is calculated from an anisotropy parameter of $\beta = 0.50$ (solid line). The dashed lines show the fits calculated from the limits of the 95% confidence interval for β.

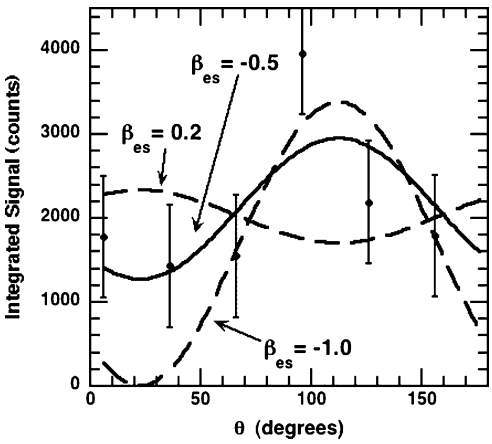

Figure 5. Angular distribution of the Cl fragments formed in the low recoil kinetic energy channel following photolysis of methyl chloroformate. The portion of the Cl signal integrated from 234 to 500 μs is plotted as a function of the lab polarization angle between the electric vector of the laser and the line from the interaction region to the detector. The integration range corresponds to the broad slow peak in each TOF distribution (e.g., see Figure 3); these C−Cl bond fission events produce excited-state methoxy carbonyl radicals. The experimental data (solid circles) are shown with $\pm\sigma$ error bars. The best fit is calculated from an anisotropy parameter of $\beta = -0.5$ (solid line). The dashed line fits are calculated from the limits of the 95% confidence interval for β, substituting $\beta = -1.0$ for the calculated limit of $\beta = -1.2$.

bond fission channel was best fit by an anisotropy parameter of $\beta = -0.5$. However, the 95% confidence interval is broad, ranging from $\beta = 0.2$ to beyond $\beta = -1$. The results for each channel are presented in Figures 4 and 5. The data indicate that the high kinetic energy channel, which yields the CH_3OCO radical in the ground electronic state, and the low kinetic energy channel, which yields electronically excited CH_3OCO, are produced from excitation to excited states with different transition dipole moments and that both dissociation channels proceed in a prompt time scale with respect to molecular rotation. This prompt dissociation would indicate that methyl

chloroformate does not undergo slow internal conversion along its dissociation pathway, but rather undergoes predissociation on excited-state potential surfaces. Indeed, the dynamics of the subsequent dissociation of the higher internal energy radicals to $CH_3O + CO$ also support the fact that the low kinetic energy radicals are not high vibrational energy ground-state radicals formed from internal conversion but rather electronically excited radicals formed via an excited-state dissociation mechanism. The fits to the $CH_3O + CO$ products from these electronically excited radicals show a high recoil kinetic energy release peaking over 25 kcal/mol (see Figure 7 in ref 15), a kinetic energy release that would not occur if these radicals were merely highly vibrationally excited radicals dissociating on the ground-state potential energy surface.

In the limit of prompt axial photofragment recoil, β can be described by eq 2, where P_2 is the second-degree Legendre polynomial and α is the angle between the transition dipole moment for the absorption and the breaking bond.[32,33] The anisotropy parameter will vary between -1, for transition dipoles perpendicular to the breaking bond, so-called perpendicular transitions, and $+2$ for transition dipoles parallel to the breaking bond, so-called parallel transitions.

$$\beta = 2P_2(\cos \alpha) \tag{2}$$

Clearly the C−Cl bond fission process resulting in ground-state radicals begins on an A′ excited state accessed via a more parallel transition moment, whereas the C−Cl bond fission events resulting in excited-state radicals begin on an A″ state accessed via a more perpendicular transition moment. We further analyze both dissociative states of methyl chloroformate in section D below.

B. Photofragment Ion Imaging Data. Imaging experiments incorporating state-selective UV photoionization found translational energy distributions roughly consistent with those presented by McCunn et al.[15] The raw images for $m/e = 35$ are shown in Figure 6. Because both the 193.3 nm photodissociation light and the 235 nm photoionization light can dissociate methyl chloroformate, the background signal was measured using only 235 nm and it was subtracted from the images obtained using both the 193.3 and 235 nm light. To reconstruct the translational energy distribution from the measured velocity distributions of state-selected Cl atoms following photoinitiated C−Cl bond fission, we sum the translational energy distributions obtained for the ground-state Cl ($^2P_{3/2}$) and excited-state Cl ($^2P_{1/2}$) atoms. Accurate reconstruction included scaling the translational energy distributions with the spin−orbit state branching ratio, $N[Cl(^2P_{1/2})]:N[Cl(^2P_{3/2})]$, given by:

$$\frac{N[C1(^2P_{1/2})]}{N[C1(^2P_{3/2})]} = k\frac{S[C1(^2P_{1/2})]}{S[C1(^2P_{3/2})]} \tag{3}$$

The experimental ion signal strengths for Cl ($^2P_{1/2}$) and Cl ($^2P_{3/2}$), $S[Cl(^2P_{1/2})]$ and $S[Cl(^2P_{3/2})]$, are measured in an alternating fashion and k is the REMPI line strength factor of 1/0.85 as measured by Liyanage et al.[34] The spin−orbit state branching ratio Cl ($^2P_{1/2}$):Cl ($^2P_{3/2}$) is 18.4:81.6. The reconstructed translational energy distribution indicates that the low kinetic energy C−Cl bond fission channel producing excited-state methoxy carbonyl radicals (A″) are formed predominantly from dissociation events that form Cl ($^2P_{3/2}$) radicals. (We do not show the reconstructed translational energy distribution because the peak E_T values were shifted by more than 3 kcal/mol from those in Figure 2 and we were only able to obtain one set of high-quality images, so were unable to check the reproducibility.) The data also indicate that the ground-state methoxy carbonyl radicals are formed with concurrent production of Cl ($^2P_{3/2}$) and Cl ($^2P_{1/2}$) atoms. Thus, the C−Cl recoil kinetic energy distribution from the imaging data is bimodal, as was the distribution observed by McCunn et al., and the state-selected images additionally reveal that the excited-state radicals formed in the low recoil kinetic energy portion of the distribution are formed in conjunction with Cl ($^2P_{3/2}$) atoms. We can also derive an anisotropy parameter for the portion of the high kinetic energy release C−Cl bond fission events that produce Cl ($^2P_{1/2}$) atoms. Integrating the high kinetic energy release Cl ($^2P_{1/2}$) signal in the top frame of Figure 6 from 160 to 360 pixels radially yields

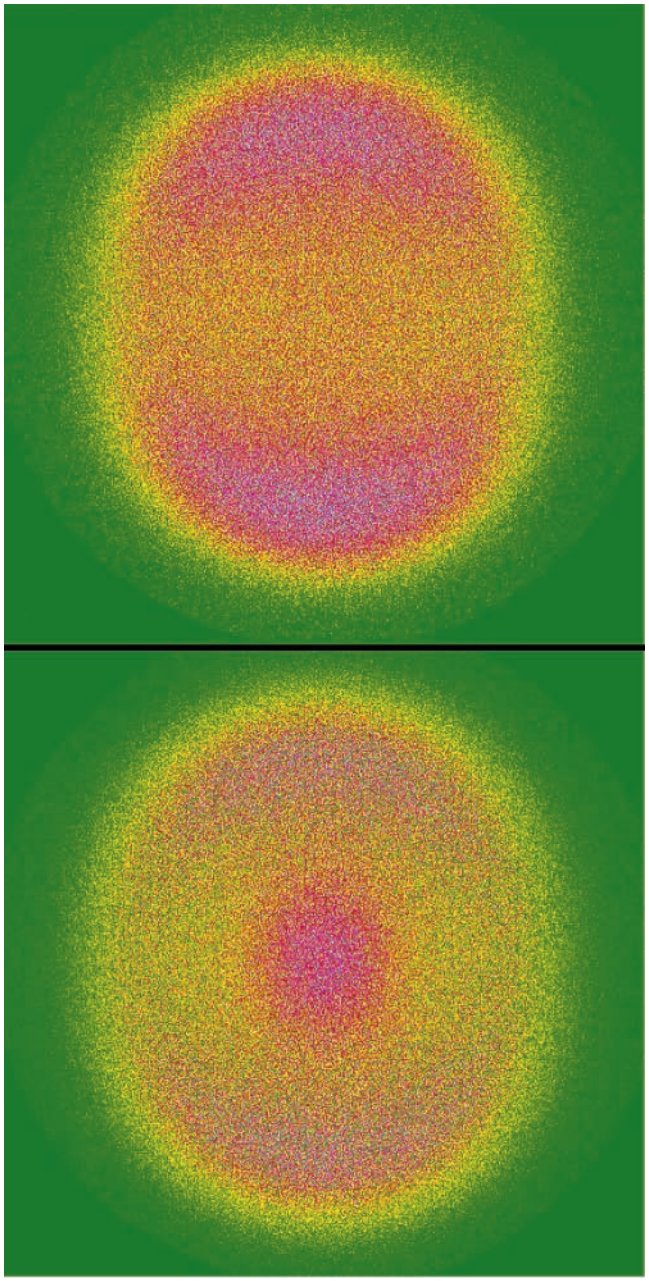

Figure 6. Raw photofragment ion images for $m/e = 35$ obtained from photolysis of methyl chloroformate at 193.3 nm. The lower image corresponds to ground-state Cl ($^2P_{3/2}$) ionized with 235.34 nm light, and the upper image corresponds to excited-state Cl ($^2P_{1/2}$) Cl atoms ionized with 235.20 nm light. The background signal for $m/e = 35$ obtained solely with 235.34 and 235.20 nm light has been subtracted from these images. The electric vector of the light is polarized in the vertical direction.

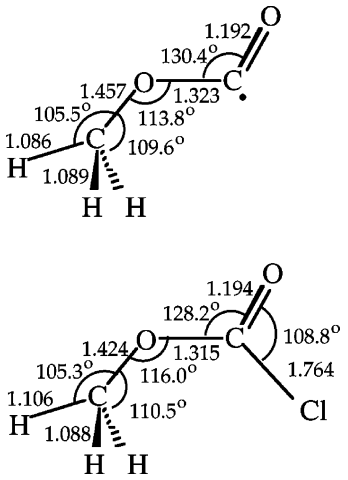

Figure 7. Ground-state UCCSD(T) equilibrium geometry for the methoxy carbonyl radical (upper diagram) conformer with a trans-geometry COCO backbone and the ground-state MC-SCF equilibrium geometry for methyl chloroformate (lower diagram) molecule with a *trans*-COCO backbone. Symmetry was not enforced during the optimization of the radical species, but to within the rounding errors used here the methoxy carbonyl radical remains symmetric. The dihedral angles for the out-of-plane H atoms are 60.5°/−60.5° and 61°/−61° for methoxy carbonyl and methyl chloroformate, respectively. All bond lengths are in angstroms, and bond angles are in degrees.

integrated signal best fit by an anisotropy parameter of $\beta = 0.72$ in good agreement with the anisotropy parameter measured for all of the high kinetic energy release C−Cl bond fission events measured with electron bombardment detection. Making a good comparison of these anisotropies relies, however, on calculating the weighted average of the Cl ($^2P_{1/2}$) and Cl ($^2P_{3/2}$) angular distributions, but determining the latter is complicated by possible alignment in the m_J distribution and its effect on the REMPI detection process. The high kinetic energy Cl ($^2P_{3/2}$) angular distribution in Figure 6, bottom, integrated from 190 to 350 pixels radially, is well-fit by the parameters (defined in ref 24, eq 2) $\beta_2 = 0.66$ and $\beta_4 = 0.02$, also evidencing a parallel angular distribution for the C−Cl bond fission events forming ground-state radicals. Determining a definitive anisotropy parameter for the low kinetic energy channel producing excited-state radicals from the imaging data is prohibited by two factors. First, these radicals are produced in conjunction with primarily only Cl ($^2P_{3/2}$), for which extracting a β parameter relies on assumptions in calculating it from the β_2 and β_4 parameters that the raw data analysis provides; and second, the angular resolution near the center of the image at these low kinetic energies is poor.

C. The Low-Lying Excited State of the CH_3OCO Radical. The ground-state equilibrium geometries of the methoxy carbonyl radical conformer and of the corresponding methyl chloroformate conformer with a *trans*-COCO backbone calculated at the UCCSD(T) and SA-MCSCF levels of theory, respectively, are reported in Figure 7. The equilibrium geometry of the methoxy carbonyl for the ground state of methyl chloroformate is similar to the geometries obtained by Groner et al.[35] and Durig and Griffin[36] in studies of methyl chloroformate's IR spectrum.

The adiabatic excitation energy of the methoxy carbonyl radical between the ground and first excited state for the conformer with the *trans*-COCO backbone is calculated at the UCCSD(T) level, giving 67.8 kcal/mol (without ΔZPE correction), which is significantly lower than the vertical excitation energy of 99.9 kcal/mol calculated by Hansen et al.[22] The UCCSD(T) value is still significantly higher than the upper bound established by the minimum internal energy of the excited-state methoxy carbonyl radical (55 kcal/mol) reported by McCunn et al.[15] The CCSD(T) method is not expected to perform well when the state of the radical has substantial multireference character, as one would expect for this radical's A″ excited state; better agreement awaits the application of higher levels of theory.

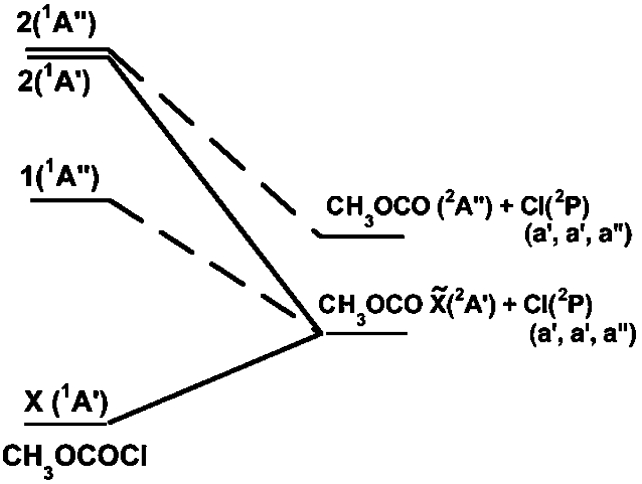

Figure 8. Correlation diagram describing the photolysis of methyl chloroformate. The A′ states are indicated by solid lines, and the A″ states are indicated by dotted lines. The energy difference between the ground state and the two highest states of methyl chloroformate shown is not drawn to scale.

D. Analysis of Photodissociation Mechanism: The Excited States of Methyl Chloroformate. We now consider whether our observed photofragment angular distributions support the assignment of the low kinetic energy C−Cl bond fission channel to producing electronically excited radicals. We note that the methoxy carbonyl radical belongs to the C_s point group and the ground state has A′ symmetry, whereas the excited state has A″ symmetry. Similarly, methyl chloroformate is in the C_s point group and has A′ symmetry in its ground state. Taking only symmetry considerations into account, we can describe the possible photodissocation routes to the methoxy carbonyl radical modeled if planar geometries are maintained along the reaction path. In the discussion below and in Figure 8, we give the possible symmetries of the Cl atom by noting the symmetry of the singly occupied p orbitals in lower case letters (a′, a′, or a″) and the total state symmetry of the methyl chloroformate reactant and radical product in capital letters. Note that if the plane of symmetry is retained then excitation of methyl chloroformate from the A′ ground state to an A″ state could yield, upon dissociation, either nascent Cl (a″) and a ground-state methoxy carbonyl radical (A′) photofragment or Cl (a′) and an excited-state methoxy carbonyl radical (A″). Excitation from the A′ ground state to an A′ excited state could produce, retaining the plane of symmetry, either nascent Cl (a″) and excited-state methoxy carbonyl radicals (A″) or Cl (a′) radicals and ground-state methoxy carbonyl (A′) radicals. These symmetry considerations in conjunction with the correlation diagram presented above allow us to interpret the observed photofragment angular distributions and the production of ground- and excited-state methoxy carbonyl radicals.

The correlation diagram, maintaining the plane of symmetry, which describes the photodissociation is presented in Figure 8. Although our preliminary MC-SCF calculations of the excited states of methyl chloroformate yielded vertical excitation energies that were far too high, they did indicate that the lowest singlet excited state of methyl chloroformate at the vertical

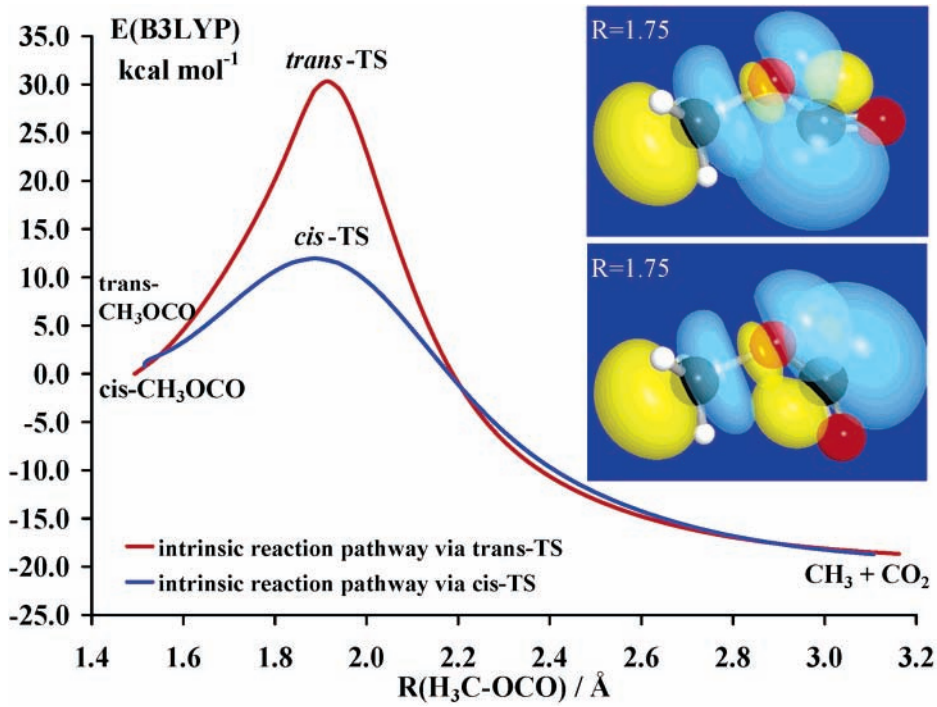

Figure 9. Energetics along the reaction coordinates for the dissociation of *cis*-/*trans*-methoxy carbonyl to $CH_3 + CO_2$ calculated at the B3LYP/6-311G(2df,p) level of theory. The energies are not zero-point-corrected. The insets in the figure are images resulting from NBO analysis of the *cis*-TS (below) and the *trans*-TS (above). The two phases of the orbitals are represented by the blue and yellow color.

TABLE 1: Calculated Dipole Transition Moments for Electronic Excitation to the Excited States of Methyl Chloroformate

excited state	⟨excited state $\|\mu_{el}\|$ X^1A'⟩ (au)	α
$2^1A'$	$0.403\mathbf{i} + 0.129\mathbf{j} + 0\mathbf{k}$ [a]	33.2°
	$0.043\mathbf{i}' + 0.343\mathbf{j}' + 0\mathbf{k}'$ [b]	46.3°
$1^1A''$	$0\mathbf{i} + 0\mathbf{j} + 0.0478\mathbf{k}$ [a]	
	$0\mathbf{i}' + 0\mathbf{j}' + 0.036\mathbf{k}'$ [b]	90.0°
$2^1A''$	$0\mathbf{i} + 0\mathbf{j} - 0.1640\mathbf{k}$ [a]	
	$0\mathbf{i}' + 0\mathbf{j}' + 0.124\mathbf{k}'$ [b]	90.0°

[a] For the conformer with the *trans*-COCO backbone, where the C−Cl bond direction is $0.941\mathbf{i} - 0.338\mathbf{j} + 0\mathbf{k}$. [b] For the conformer with the *cis*-COCO backbone, where the C−Cl bond direction is $0.804\mathbf{i}' - 0.595\mathbf{j}' + 0\mathbf{k}'$.

geometry was of A″ symmetry, labeled $1^1A''$ in Figure 8. They also indicated that at higher excitation energies there were two energetically close (at the vertical geometry) singlet excited states, one of A′ symmetry, labeled $2^1A'$ in Figure 8 and Table 1, and one of A″ symmetry, labeled $2^1A''$ in Figure 8 and Table 1. Because some of our photofragments evidence a parallel angular distribution and some had a perpendicular angular distribution, we conclude that electronic excitation at 193 nm accesses these two closely lying excited states of methyl chloroformate. The correlation diagram then indicates which products you would expect upon excitation to each of these higher energy electronic states if you restrict the dynamics to geometries with a plane of symmetry. Excitation from the X $^1A'$ ground state to the $2^1A'$ state (a parallel transition moment in both molecular conformers as shown in Table 1) would yield Cl atoms with a singly occupied a′ orbital and ground-state methoxy carbonyl (X $^2A'$) upon dissociation in planar geometry. Excitation from the X $^1A'$ ground state to the to the 2 $^1A''$ state (a perpendicular transition moment) gives the first state to correlate to excited state, $^2A''$, radical products in planar geometries (the Cl atom co-fragment would have one unpaired electron in an a′ orbital.) Qualitatively, these results are in good agreement with our angular distribution data that determined a mostly parallel transition for the formation of ground-state methoxy carbonyl radical and a mostly perpendicular transition for the formation of excited-state methoxy carbonyl radical. Of course, in nonplanar geometries the $2^1A'$ state and the $2^1A''$ states mix, so one would expect the angular distribution of the products to be of mixed character. There are also triplet states in this energy region that may play a role in the dissociation dynamics. Nevertheless, the zeroth-order planar correlation diagram does qualitatively rationalize our observed angular distributions and strongly supports the assignment of the low kinetic energy C−Cl bond fission channel to one that produces electronically excited radical coproducts.

E. Unimolecular Dissociation of the Methoxy Carbonyl Radical: Natural Bond Orbital Computations. We now seek to understand why, as mentioned before, the methoxy carbonyl radical product encounters a much higher barrier via the trans-geometry transition state to form CH_3 and CO_2 than it does via the *cis*-TS. The dramatically lower energy of the cis barrier is strongly supported by the large branching to that channel observed experimentally by McCunn et al.[15] The potential energy surfaces of the dissociation pathways for ground-state *cis*-/*trans*-methoxy carbonyl to form the methyl radical and carbon dioxide are plotted in Figure 9. The potential energy is set relative to the minimum of *trans*-methoxy carbonyl, and the computations are not zero-point-corrected. Except for the different orientation of the methyl group relative to the terminal carbonyl group, in fact, the *cis*-TS and the *trans*-TS have very similar geometries at the B3LYP/6-311G(2df,p) and CCSD(T)/6-311G(2df,p) levels.[15] One may postulate that the lower energy profile for dissociation via the *cis*-TS could be attributed to a bonding feature exclusively present on the cis pathway. From the NBO analysis along the pathway between the *cis*-methoxy carbonyl and the *cis*-TS, we found that there is a strong stabilization effect due to the donation of electron density from the nonbonding C orbital into the σ^* orbital of the methoxy C−O bond ($n_C \rightarrow \sigma^*_{CO}$). The stabilization energy (or energy

TABLE 2: $E(2)$ Term for the $n_C \rightarrow \sigma^*_{CO}$ Interaction, the Orbital Energy Difference [$E(\sigma^*_{CO}) - E(n_C)$], the Off-Diagonal NBO Fock Matrix Element [$F(n_C,\sigma^*_{CO})$], and the Contribution of the Leading Resonance Structure along the Intrinsic Reaction Coordinates from $R = 1.46$ to 1.84 Å

$R(H_3C-OCO)$ (Å)	$E(2)$ $n_C \rightarrow \sigma^*_{CO}$ [a] (kcal/mol)	$E(\sigma^*_{CO}) - E(n_C)$ (hartree)	$F(n_C,\sigma^*_{CO})$ (hartree)	contribution[b]
1.46	8.4	0.55	0.086	78.0
1.49	10.4	0.51	0.092	62.5
1.60	14.1	0.41	0.096	58.9
1.70	22.0	0.32	0.106	52.9
1.75	27.5[c]	0.18[c]	0.091[c]	19.7
1.84	58.7[c]	0.13[c]	0.109[c]	12.6

[a] $E(2)$ is defined as $F(n_C,\sigma^*_{CO})^2/[E(\sigma^*_{CO}) - E(n_C)]$. [b] Contribution of the leading resonance structure obtained in the natural resonance theory analysis. [c] Values are obtained from choosing the reactant-like resonance structure in the NBO analysis.

lowering) is characterized as the $E(2)$ term in a second-order perturbation theory treatment in the NBO program.[28,29] The $E(2)$ term (in kcal/mol) along the IRC between the *cis*-methoxy carbonyl and the *cis*-TS is found to increase with bond length R_{c-o}: $E(2) = 8.4$ ($R_{c-o} = 1.46$ Å, i.e., *cis*-methoxy carbonyl), 10.4 ($R_{c-o} = 1.49$ Å), 14.1 ($R_{c-o} = 1.60$ Å), 22.0 ($R_{c-o} = 1.70$ Å), 27.5 ($R_{c-o} = 1.75$ Å), and 58.7 ($R_{c-o} = 1.84$ Å). Negligible stabilization was found on the *trans*-methoxy carbonyl IRC. The donor interaction from the nonbonding C orbital to the σ^* orbital of the H_3C-OCO bond greatly stabilizes the dissociation of the *cis*-methoxy carbonyl via *cis*-TS, which leads to the methyl + CO_2 product channel. Such hyperconjugative donor−acceptor interactions are known to have stereoelectronic preference for donor and acceptor orbitals in vicinal antiperiplanar orientation,[37] as can only occur here in the cis isomer. Alternatively, in the trans isomer the corresponding n_C, σ^*_{CO} NBOs are in syn-periplanar orientation, with donor oxygen lone pairs anti to the n_C orbital. The corresponding $n_C \rightarrow \sigma^*_{CO}$ stabilization is therefore essentially absent along the trans dissociation pathway, leading to a much higher energy profile than that for the favored cis dissociation pathway. The insets in Figure 9 are NBO renderings of the nonbonding C orbital and the σ^* orbital of methoxy CO bond at a geometry in vicinity of the corresponding *cis*-TS ($R_{c-o} = 1.75$ Å) and *trans*-TS ($R_{c-o} = 1.75$ Å). In the cis configuration, there is clearly a large overlap between the nonbonding C orbital and the σ^* orbital. However, in the trans configuration the overlap between the nonbonding C orbital and the σ^* orbital is minimal, in part due to the changing phase of the σ^* orbital where it overlaps the nonbonding C orbital.

Table 2 shows the $E(2)$ energy lowering, the orbital energy difference [$E(\sigma^*_{CO}) - E(n_C)$], the off-diagonal NBO Fock matrix element [$F(n_C,\sigma^*_{CO})$], and the contribution of the leading resonance structure at different value of $R(H_3C\text{-}OCO)$. The $E(2)$ energy is defined as in eq 4:[28,29]

$$E(2) = \frac{[F(n_C,\sigma^*_{CO})]^2}{[E(\sigma^*_{CO}) - E(n_C)]} \tag{4}$$

As the bonding distance between the CH_3 and OCO moieties increases from 1.46 to 1.70 Å, the orbital energy difference becomes smaller and smaller because of the zeroth-order energy lowering of the σ^*_{CO} orbital of the breaking CO bond. The off-diagonal NBO Fock matrix element is also increased from 0.086 to 0.106 au. Both effects contribute to the increase of the $E(2)$ term with the $R(H_3C-OCO)$, but the former effect due to orbital energy difference (in the denominator of the $E(2)$ expression) is more significant. The last column in Table 2 shows a noticeable trend that the contribution of the leading reactant resonance structure ($CH_3-O-\dot{C}=O$) is decreased as one moves away from the equilibrium geometry of the radical toward the transition state. The contribution dropped from 78% at $R = 1.46$ Å to about 53% at $R = 1.70$ Å, nearing the TS. For displacements along the reaction coordinate from $R = 1.75$ to 1.85 Å the contributions of this reactant-like resonance structure dropped sharply below 20%. Over that region of the reaction coordinate, the dominant resonance structure is found to be that of dissociation product $CH_3 + CO_2$ species, which makes the perturbative evaluation of the $E(2)$ term in terms of $CH_3-O-\dot{C}=O$ "unperturbed" NBOs increasingly inappropriate. In spite of this, we have intentionally enforced a 100% contribution of the $CH_3-O-\dot{C}=O$ resonance structure to the NBO analysis along the reaction coordinate where $R = 1.75$ Å and 1.84 Å to show the continuity of the reactant-like NBO description even past the TS and into the product region. This establishes the qualitative applicability of the $n_C \rightarrow \sigma^*_{CO}$ hyperconjugative picture over the relevant portion of the IRC. Thus, the NBO analysis gives important qualitative insight into the relative energetic difference between the *cis*-TS and the *trans*-TS (the *cis*-TS is more stable than the *trans*-TS by ~20 kcal/mol at the CCSD(T) level[15]) explaining the substantial branching to the $CH_3 + CO_2$ product channel observed by McCunn et al.

F. Correcting the Branching Fractions for Producing Excited-State and Ground-State Radicals. As noted above, we calculated a corrected branching ratio for production of ground-state and excited-state methoxy carbonyl radicals from the photodissociation of methyl chloroformate at 193.3 nm using the photofragment angular distribution data. McCunn et al. 's results[15] yielded 0.85:0.15 as the ratio, but the author's analysis of products assumed that both C−Cl bond fission events had the same angular dependence and, therefore, did not account for the fact that photofragments produced via parallel transitions are overcounted due to the experimental geometry of the crossed laser-molecular beam experiments. The correct branching ratio is calculated using eq 5:

$$\frac{\sigma_{\text{ground state}}}{\sigma_{\text{excited state}}} = \left[\frac{\sigma^o_{gs}}{\sigma^o_{es}}\right]\left[\frac{1+\frac{\beta_{es}}{4}}{1+\frac{\beta_{gs}}{4}}\right] \tag{5}$$

Using McCunn's empirical product branching ratio[15] for the σ^o ratio, $\beta_{gs} = 0.50$ and $\beta_{es} = -0.5$ in eq 5 yields our product branching ratio of 0.82:0.18.

IV. Conclusions

There are two particularly interesting results in this work. The natural bond orbital analysis along the two $CH_3OCO \rightarrow CH_3 + CO_2$ reaction coordinates yielded a simple physical picture to understand why the dissociation pathway via the cis transition state encounters a much lower barrier than that via the trans transition state. We trust that it will help guide other

workers as they seek to identify all of the important transition states on complex polyatomic potential energy surfaces. The stability of the cis dissociation pathway compared to the trans dissociation pathway that is exhibited by methoxy carbonyl radicals is also present in the dissociation of HOCO to produce $H + CO_2$,[38] where the *cis*-TS is calculated to be 6.4 kcal/mol lower in energy than the *trans*-TS. Presumably, the stability of the HOCO *cis*-TS can be explained by a similar acceptor−donor relationship; however, in the CH_3OCO radical the energy lowering $E(2)$ along the cis-geometry reaction coordinate is much more significant, presumably because the energy of the σ^*(C−O) orbital as the C−O bond stretches along the reaction coordinate brings it energetically closer to the n_C natural orbital, resulting in a stronger interaction.

The anisotropy measurements, complemented by theoretical analysis, in this study support the assignment of the minor low recoil kinetic energy C−Cl bond fission channel observed in the photodissociation of methyl chloroformate to one producing the A″ low-lying excited state of the methoxy carbonyl radical. However, the calculated adiabatic excitation energy of the radical is somewhat higher than the upper limit calculated from the experimental data. Thus, this study also represents a benchmark for further excited-state electronic structure calculations on this radical and others with substantial multireference character in the excited state.

Acknowledgment. This work was supported by the Chemical, Geosciences and Biosciences Division, Office of Basic Energy Sciences, Office of Science, U.S. Department of Energy, under Grant No. DE-FG02-92ER14305. M.J.B. acknowledges support from a Jean Dreyfus Boissevain Undergraduate Scholarship for Excellence in Chemistry. D.I.G.B. acknowledges the support of the Arnold and Mebel Beckman Foundation. We thank R. Ismagilov for encouraging us to pursue the NBO analysis within.

Note Added in Proof. Using Fieller's method (Fieller, E.C. *J.R. Stat. Soc., Ser. B* **1954**, *16*, 175−185.), we calculated and added to the text the 95% confidence intervals for the measured anisotropy parameters. We thank P. McCullagh, M. Wang, and M. Stein for their patient tutoring on this method.

References and Notes

(1) Francisco, J. S. *Chem. Phys.* **1998**, *237*, 1.

(2) Steinfeld, J. I.; Francisco, J. S.; Hase, W. L. *Chemical Kinetics and Dynamics*; Prentice Hall, Inc.: Upper Saddle River, NJ, 1989.

(3) Seinfeld, J. H.; Pandis, S. N. *Atmos. Chem. Phys.*: *From Air Pollution to Climate Change*; John Wiley & Sons, Inc.: New York, 1998.

(4) Good, D. A.; Hanson, J.; Francisco, J. S.; Li, Z.; Jeong, G.-R. *J. Phys. Chem. A* **1999**, *103*, 10893.

(5) Good, D. A.; Francisco, J. S. *J. Phys. Chem. A* **2000**, *104*, 1171.

(6) Glaude, P. A.; Pitz, W. J.; Thomson, M. J. *Proc. Combust. Inst.* **2005**, *30*, 1111.

(7) Wallington, T. J. H.; Hurley, M. D.; Maurer, T.; Barnes, I.; Becker, K. H.; Tyndall, G. S.; Orlando, J. J.; Pimentel, A. S.; Bilde, M. *J. Phys. Chem. A* **2001**, *105*, 5146.

(8) Good, D. A.; Hansen, J.; Kamoboures, M.; Santiono, R.; Francisco, J. S. *J. Phys. Chem. A* **2000**, *104*, 1505.

(9) Wallington, T. J.; Dagaut, P.; Liu, R.; Kurylo, M. *Int. J. Chem. Kinet.* **1988**, *20*, 177.

(10) Good, D. A.; Francisco, J. S. *J. Phys. Chem. A* **2002**, *106*, 1733.

(11) Le Clave, S.; Le Bras, G.; Mellouki, A. *J. Phys. Chem. A* **1997**, *102*, 5489.

(12) Kang, J. K.; Musgrave, C. B. *J. Chem. Phys.* **2001**, *115*, 11040.

(13) Wang, B.; Hou, H.; Gu, Y. *J. Phys. Chem. A* **1999**, *103*, 8021.

(14) Zhou, Z. Y.; Cheng, X. L.; Zhou, X. M.; Fu, H. *Chem. Phys. Lett.* **2002**, *353*, 281.

(15) McCunn, L. R.; Lau, K.-C.; Krisch, M. J.; Butler, L. J.; Tsung, J. W.; Lin, J. J. *J. Phys. Chem. A* **2006**, *110*, 1625.

(16) Beckwith, A. L. J.; Bowry, V. W. *J. Am. Chem. Soc.* **1994**, *116*, 2710.

(17) Simakov, P. A.; Martinez, F. N.; Horner, J. H.; Newcomb, M. *J. Org. Chem.* **1998**, *63*, 1226.

(18) Bucher, G.; Halupka, M.; Kolano, C.; Schade, O.; Sander, W. *Eur. J. Org. Chem.* **2001**, 545.

(19) Morihovitis, T.; Schiesser, C. H.; Skidmore, M. A. *J. Chem. Soc., Perkin Trans.* **1999**, *2*, 2041.

(20) Zhu, L.; Bozzelli, J. W. *Theochem.* **2005**, *728*, 147.

(21) Westbrook, C. K.; Pitz, W. J.; Curran, H. J. *J. Phys. Chem A* **2006**, *110*, 6912.

(22) Hansen, J. C.; Li, Y.; Francisco, J. S.; Szente, J. J.; Maricq, M. M. *J. Chem. Phys.* **2000**, *113*, 6465.

(23) Morton, M. L.; Szpunar, D. E.; Butler, L. J. *J. Chem. Phys.* **2001**, *115*, 204.

(24) Liu, Y; Butler, L. J. *J. Chem. Phys.* **2004**, *121*, 11016.

(25) Lau, K.-C.; Liu, Y.; Butler, L. J. *J. Chem. Phys.* **2005**, *123*, 54322.

(26) Dribiniski, V.; Ossadtchi, A.; Mandelshtam, V. A.; Reisler, H. *Rev. Sci. Instrum.* **2002**, *73*, 2634.

(27) Werner, H.-J.; Knowles, P. J.; Lindh, R.; Manby, F. R.; Schütz, M.; Celani, P.; Korona, T.; Rauhut, G.; Amos, R. D.; Bernhardsson, A.; Berning, A.; Cooper, D. L.; Deegan, M. J. O.; Dobbyn, A. J.; Eckert, F.; Hampel, C.; Hetzer, G.; Lloyd, A. W.; McNicholas, S. J.; Meyer, W.; Mura, M. E.; Nicklass, A.; Palmieri, P.; Pitzer, R.; Schumann, U.; Stoll, H.; Stone, A. J.; Tarroni, R.; Thorsteinsson, T. *MOLPRO*, a package of ab initio programs.

(28) Foster, J. P.; Weinhold, F. *J. Am. Chem. Soc.* **1980**, *102*, 7211−7218.

(29) Reed, A. E.; Curtiss, L. A.; Weinhold, F. *Chem. Rev.* **1988**, *88*, 899−926.

(30) Weinhold, F. Natural Bond Orbital Methods. In *Encyclopedia of Computational Chemistry*; Schleyer, P. v. R., Allinger, N. L., Clark, T., Gasteiger, J., Kollman, P. A., Schaefer, H. F., III, Schreiner, P. R., Eds.; John Wiley & Sons: Chichester, U.K., 1998; Vol. 3, pp 1792−1811.

(31) Glendening, E. D.; Badenhoop, J. K.; Reed, A. E.; Carpenter, J. E.; Bohmann, J. A.; Morales, C. M.; Weinhold, F. *NBO 5.0*. Theoretical Chemistry Institute, University of Wisconsin, Madison, 2001. www.chem.wisc.edu/∼nbo5.

(32) Zare, R. N. *Mol. Photochem.* **1973**, *4*, 1.

(33) Busch, G. E.; Wilson, K. R. *J. Chem. Phys.* **1972**, *56*, 3638.

(34) Liyanage, R.; Yang, Y. A.; Hashimoto, S.; Gordon, R. J.; Field, R. W. *J. Chem. Phys.* **1995**, *103*, 6811.

(35) Groner, P.; Tolly, C. L.; Durig, J. R. *Chem. Phys.* **1990**, *142*, 381.

(36) Durig, J. R.; Griffin, M. G. *J. Mol. Spectrosc.* **1977**, *64*, 252.

(37) Weinhold, F.; Landis, C. R. *Valency and Bonding: A Natural Bond Orbital Donor-Acceptor Perspective*; Cambridge Univ. Press: Cambridge, U.K., 2005.

(38) Yu, H.-G.; Muckerman, J. T.; Sears, T. J. *Chem. Phys. Lett.* **2001**, *349*, 547. The energy difference is 7.55 kcal/mol with zero-point correction.